Article:

Mist, J., Andel, B., Andreyev, A. N. orcid.org/0000-0003-2828-0262 et al. (61 more authors) (2025) β- and α-decay spectroscopy of 182Au. Phys. Rev. C. 024328. ISSN: 2469-9993

https://doi.org/10.1103/rf8d-v286

β- and α-decay spectroscopy of ^{182}Au

J. Mišt,[1,*] B. Andel,[1] A. N. Andreyev,[2,3] A. E. Barzakh,[4] J. G. Cubiss,[2,†] A. Algora,[5,6] S. Antalic,[1] M. Athanasakis-Kaklamanakis,[7] M. Au,[7] S. Bara,[8] R. A. Bark,[9] M. J. G. Borge,[10] A. Camaiani,[8,11,12] K. Chrysalidis,[7] T. E. Cocolios,[8] C. Costache,[13] H. De Witte,[8] R. Y. Dong,[14] D. V. Fedorov,[4] V. N. Fedosseev,[7] L. M. Fraile,[15] H. O. U. Fynbo,[16] R. Grzywacz,[17] R. Heinke,[7] C. F. Jiao,[14] J. Johnson,[8] P. M. Jones,[9] D. S. Judson,[18] D. T. Kattikat Melcom,[19] M. M. Khan,[8,20] J. Klimo,[8] A. Korgul,[21] M. Labiche,[22] R. Lică,[13] Z. Liu,[23] M. Madurga,[17] N. Marginean,[13] P. Marini,[19,‡] B. A. Marsh,[7,§] C. Mihai,[13] P. L. Molkanov,[4] E. Nácher,[5] C. Neacsu,[13] J. N. Orce,[24] R. D. Page,[18] J. Pakarinen,[25,28] P. Papadakis,[22] S. Pascu,[13] A. Perea,[10] M. Piersa-Siłkowska,[21] Zs. Podolyák,[26] M. D. Seliverstov,[4] A. Sitarčík,[1] E. Stamati,[7,27] A. Stoica,[13] A. Stott,[2] M. Stryjczyk,[25,28,29] O. Tengblad,[10] I. Tsekhanovich,[19] A. Turturica,[13] J. M. Udías,[15] P. Van Duppen,[8] N. Warr,[30] and A. Youssef[8]

(ISOLDE Decay Station Collaboration)

[1]*Department of Nuclear Physics and Biophysics, Comenius University in Bratislava, 84248 Bratislava, Slovakia*
[2]*School of Physics, Engineering and Technology, University of York, York YO10 5DD, United Kingdom*
[3]*Advanced Science Research Center, Japan Atomic Energy Agency, Tokai-mura, Ibaraki 319-1195, Japan*
[4]*Affiliated with an institute covered by a cooperation agreement with CERN at the time of the experiment*
[5]*Instituto de Física Corpuscular, CSIC-Universidad de Valencia, E-46071 Valencia, Spain*
[6]*Institute of Nuclear Research (ATOMKI), P.O.Box 51, H-4001 Debrecen, Hungary*
[7]*CERN, CH-1211 Geneve 23, Switzerland*
[8]*KU Leuven, Instituut voor Kern- en Stralingsfysica, 3001 Leuven, Belgium*
[9]*iThemba LABS, National Research Foundation, P. O. Box 722, Somerset West 7129, South Africa*
[10]*Instituto de Estructura de la Materia, CSIC, 28006 Madrid, Spain*
[11]*Dipartimento di Fisica, Università di Firenze, I-50019 Sesto Fiorentino, Italy*
[12]*Istituto Nazionale di Fisica Nucleare, Sezione di Firenze, I-50019 Sesto Fiorentino, Italy*
[13]*Horia Hulubei National Institute of Physics and Nuclear Engineering (IFIN-HH), R-077125 Bucharest, Romania*
[14]*School of Physics and Astronomy, Sun Yat-sen University, Zhuhai 519082, China*
[15]*Grupo de Física Nuclear and IPARCOS, Universidad Complutense de Madrid, CEI Moncloa, E-28040 Madrid, Spain*
[16]*Department of Physics and Astronomy, Aarhus University, DK-8000 Aarhus C, Denmark*
[17]*Department of Physics and Astronomy, University of Tennessee, Knoxville, Tennessee 37966, USA*
[18]*Oliver Lodge Laboratory, University of Liverpool, Liverpool, L69 7ZE, United Kingdom*
[19]*Univ. Bordeaux, CNRS, LP2I, UMR 5797, F-33170 Gradignan, France*
[20]*IMT Atlantique, Nantes Université, CNRS-IN2P3, Nantes, France*
[21]*Faculty of Physics, University of Warsaw, PL 02-093 Warsaw, Poland*
[22]*STFC Daresbury Laboratory, Daresbury, WA4 4AD Warrington, United Kingdom*
[23]*Institute of Modern Physics, Chinese Academy of Sciences, Lanzhou 730000, China*
[24]*Department of Physics, University of the Western Cape, P/B X17 Bellville 7535, South Africa*
[25]*Accelerator Laboratory, Department of Physics, University of Jyväskylä, P.O. Box 35, FI-40014, University of Jyväskylä, Finland*
[26]*Department of Physics, University of Surrey, Guildford GU2 7XH, United Kingdom*
[27]*University of Ioannina, P.O. Box: 1186, Ioannina, Epirus, Greece*
[28]*Helsinki Institute of Physics, University of Helsinki, FI-00014 Helsinki, Finland*
[29]*Institut Laue-Langevin, 71 Avenue des Martyrs, F-38042 Grenoble, France*
[30]*Institut für Kernphysik, Universität zu Köln, Köln D-50937, Germany*

(Received 26 May 2025; accepted 21 July 2025; published 28 August 2025)

*Contact author: jozef.mist@fmph.uniba.sk
†Present address: School of Physics and Astronomy, University of Edinburgh, Edinburgh, EH9 3FD, United Kingdom.
‡Present address: Grand Accélérateur National d'Ions Lourds, CNRS/IN2P3-CEA/DRF, 14000 Caen, France.
§Deceased.

An α- and β-decay study of a pure source of laser-ionized and mass-separated ^{182}Au ($Z = 79$, $N = 103$) was carried out at the ISOLDE Decay Station at the ISOLDE-CERN facility. Detailed γ-γ analysis following EC/β^+ decay of ^{182}Au was performed, and the level scheme of daughter nuclide ^{182}Pt was considerably extended via the identification of 125 new levels and 336 new γ-ray transitions. The nonexistence of a relatively long-lived isomeric state in ^{182}Au and influence of the pandemonium effect on β-decay feeding intensities are discussed. Differences in feeding for two coexisting bands in ^{182}Pt were investigated. The α-decay scheme of ^{182}Au was extended and an α-decay branching ratio of 0.129(11)% was measured. Hindrance factors for α-decay branches were calculated and $I^\pi = (1^+, 2^+, 3^+)$ assignment for the ^{178}Ir ground state was proposed.

DOI: 10.1103/rf8d-v286

I. INTRODUCTION

Neutron-deficient gold ($Z = 79$) nuclei manifest various ground state (g.s.) shapes along the isotopic chain. A sudden shift from nearly spherical ground states in ^{187}Au ($N = 108$) and heavier isotopes to a strongly deformed prolate shape in $^{183-186}$Au ($N = 104$–107) has been known since the 1970s [1–4]. Recent laser spectroscopy studies [5–9] extended the systematics of changes in mean-squared charge radii up to ^{176}Au ($N = 97$). The trend of strong g.s. deformation was observed to continue in $^{180-182}$Au, whereas the ground states of ^{176,177,179}Au return back to the spherical trend, similarly to $A \geqslant 187$ gold isotopes [5,9]. Shape coexistence in gold isotopes has also been confirmed by extensive in-beam and decay spectroscopy studies [10–16].

Electron capture (EC)/β^+-decay studies of gold isotopes allow for probing the shape coexistence in the daughter platinum ($Z = 78$) nuclei. The systematics of low-lying levels in the neutron-deficient platinum isotopes around $N = 104$ show two coexisting configurations [17–19]. Ground states of ^{188}Pt and heavier isotopes are weakly oblate, while the prolate configuration state lies higher in energy. However, for $^{178-186}$Pt, the strongly deformed configuration becomes the g.s., see Fig. 57 in Ref. [19]. Platinum nuclei have also been investigated in several in-beam spectroscopy studies, producing information on a coexistence of two bands [20–25].

^{182}Au and its EC/β^+ decay daughter ^{182}Pt have been the main focus of several α- and β-decay spectroscopy studies in the past [26–30]. The nuclide ^{182}Au has a dominant β-decay branch ($b_\beta = 99.87(5)\%$ [30], $b_\beta = 99.962(8)\%$ [31] and $b_\beta \approx 99.96\%$ [26]) and an evaluated half-life of $T_{1/2} = 15.5(4)$ s [32]. Only one long-lived state is known in ^{182}Au. Its spin and parity $I^\pi = (2^+)$ was first proposed in the nuclear orientation [33] and decay spectroscopy [34] studies and further confirmed by the laser spectroscopy measurement of the hyperfine structure [6]. However, a 5^- isomer in ^{182}Au was proposed in the recent NUBASE evaluation [35].

In the latest β-decay study, the ^{182}Au nuclei were produced in a fusion-evaporation reaction ^{149}Sm(^{37}Cl, $4n$) ^{182}Au at the Australian National University [36]. Several low-spin excited states in ^{182}Pt were identified up to an excitation energy of $\approx$1.9 MeV. The spin and parity I^π assignment for several nonyrast states was based on γ-γ angular correlation and conversion coefficient measurements. In the same study, a band-mixing model was applied to low-lying yrast and nonyrast states, showing mixing between a less and a more deformed band together with the γ-vibration band.

In the present paper, we report on the investigation of excited states in ^{182}Pt and ^{178}Ir via EC/β^+ decay and α decay, respectively, of the pure sample of laser-ionized and mass-separated ^{182}Au. A large quantity of spectroscopic data have been obtained, allowing the extension of both ^{182}Au β- and α-decay schemes. The β-decay feeding intensities and hindrance factors were evaluated, and the obtained results are discussed.

II. EXPERIMENT

The experiment was performed at the ISOLDE facility at CERN [37]. Nuclei of ^{182}Au were produced in spallation reactions induced by a 1.4-GeV proton beam impinging onto a 50-g/cm^2-thick UC$_x$ target. The beam provided by the Proton Synchrotron Booster consisted of 2.4-µs-long pulses with a repetition time of 1.2 s grouped into a so-called supercycle consisting of around 25 pulses. Because of the high production rate, only two proton pulses from each supercycle were used. The average beam intensity was $\approx$0.17 µA. Additionally, to avoid saturating the detection system, the intensity of ^{182}Au was further reduced by opening the ISOLDE beam gate only for 2 s with a delay of 0.4 s after the impact of each proton pulse.

Produced nuclei diffused through the target heated to $\approx$2000 °C and effused towards the hot cavity of Resonance Ionization Laser Ion Source (RILIS) [38] through the transfer line. Gold atoms were selectively ionized inside this cavity using a three-step resonance ionization scheme by laser beams with wavelengths of 267.6, 306.5, and 673.9 nm (see Fig. 6 in Ref. [6]). Ions were extracted from the ion source by a 30-kV electrostatic potential and sent through the General Purpose Separator, separating them with respect to their mass-to-charge ratio $A/q = 182$. The combination of selective laser ionization and mass separation allowed a high-purity sample of ^{182}Au to be obtained.

The beam of ^{182}Au was implanted into a movable aluminized mylar tape placed inside a vacuum chamber of the ISOLDE Decay Station (IDS) [39]. The tape was automatically moved every supercycle (approximately every 30 s) to remove long-lived daughter activities. Inside the vacuum chamber, close to the implantation point, an array of seven silicon PIN diodes with a thickness of 300 µm was placed to measure conversion electrons and α particles. It consisted of one 15×15 mm^2 detector and six 7×7 mm^2 detectors placed above and below the larger one. Four HPGe Clover detectors for γ-ray detection and two plastic scintillators for β-particle detection were placed outside the vacuum chamber.

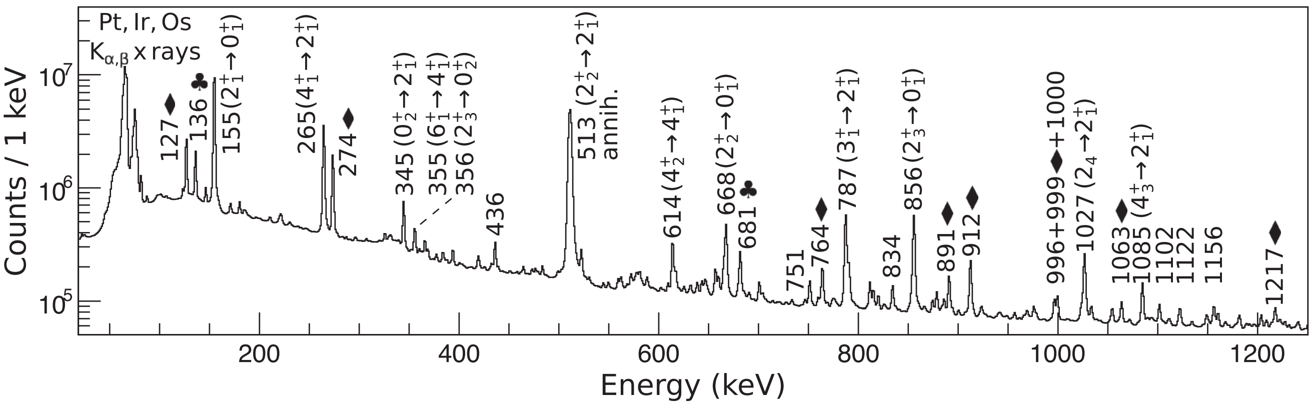

FIG. 1. Singles γ-ray spectrum from the measurement of ^{182}Au. Peak energies are labeled in keV. Transitions following EC/β^+ decay of ^{182}Au have no special symbol, transitions labeled with (♣) and (♦) follow EC/β^+ decays of ^{182}Pt and ^{182}Ir, respectively. These isobars were produced in the β decay of ^{182}Au only; no direct production was possible. The remaining part of the spectrum is shown in Fig. 1 in Supplemental Material [40].

Energy calibration of HPGe detectors was performed using ^{152}Eu, ^{60}Co, ^{137}Cs, and ^{241}Am sources. The resulting energy resolution using add-back for four crystals within the same Clover detector was 2.4 keV for 1085-keV (full width at half maximum) and 3.7 keV for 3094-keV transitions in ^{182}Pt. The absolute detection efficiency calibration was performed with ^{152}Eu and ^{241}Am sources of known activity.

The α-particle detection efficiency of the silicon array was obtained using the known α(5479 keV)-γ(148 keV) coincidence in ^{181}Au α decay, which was measured during the same experiment. The comparison of the number of 148-keV γ rays from the singles γ-ray spectrum and from the α-γ coincidences gated on the 5479-keV α line [30] resulted in the α-particle detection efficiency of 3.8(4)%. This value was reproduced by a GEANT4 simulation, which was then used to obtain the detection efficiency curve for conversion electrons. The energy resolution of the silicon array was 11 and 24 keV for conversion electrons (at 377 keV) and α particles (at 5870 keV), respectively. All signals from the detectors were recorded in a triggerless mode using the Pixie-16 250 MHz [41] digital data acquisition system.

III. RESULTS

A. Introduction to the data analysis

A singles γ-ray spectrum with labeled known transitions following the β decay of ^{182}Au and decays of its daughter products is shown in Fig. 1. Based on the number of counts of the 154.9-keV γ ray ($2_1^+ \to 0_1^+$ transition in ^{182}Pt), corrected for the γ-ray detection efficiency and absolute transition intensity of 43.8(9) per 100 β decays determined in this work (see Sec. III D), there were about $3.3(1) \times 10^8$ β decays of ^{182}Au nuclei in the chamber. A small contamination from the β decay of surface-ionized ^{182}Tl was observed and its amount ($\approx 1.7 \times 10^5$ β decays) was estimated in the same way using the 351-keV[1] γ-ray transition in ^{182}Hg [42].

The γ rays belonging to ^{182}Pt were identified using the γ-γ coincidences with previously known transitions and with platinum $K_{\alpha,\beta}$ x rays. The prompt coincidence time window between two signals was set to 200 ns. Background subtraction of coincidence spectra was performed by gating on the close region on both sides of the peak of interest. Coincidence γ-ray spectra gated on the 154.9-keV $2_1^+ \to 0_1^+$ and 264.6-keV $4_1^+ \to 2_1^+$ transitions are shown in Figs. 2 and 3.

We note that in the case of transitions observed both in our work and Ref. [36], our energies are systematically lower. The differences are usually around 0.5 keV and up to 1 keV for the 1386-keV transition deexciting the level at 1541 keV. To test our calibration, we compared the measured energies of the natural background radiation and γ rays from ^{182}Au decay chain with the literature values. The differences were within 0.2 keV for ^{40}K (1460.851 keV) [43] and ^{182}Ir (273.5 and 912.1 keV) [32], and within 0.3 keV for ^{214}Bi (1764.491 keV) [44] and ^{208}Tl (2614.511 keV) [45] from their tabulated values.

Relative intensities of transitions following the ^{182}Au β decay were determined from the singles γ-ray spectrum where possible; otherwise, they were deduced from γ-γ coincidences. For selected intense γ rays, for which contamination was ruled out, there was a discrepancy of up to 12% in intensities obtained by both approaches. The most probable cause is γ-γ angular correlations. Because of the unknown multipolarity of most transitions, a correction was not possible, therefore, an additional uncertainty of 12% was added to intensities obtained from γ-γ coincidences (see Table I). Intensities were normalized to the most intense 155-keV line in ^{182}Pt. A correction for the summing of γ-rays in cascades was performed.

[1]The absolute intensity of ∼76 per 100 decays was estimated from published transition intensities from Ref. [42].

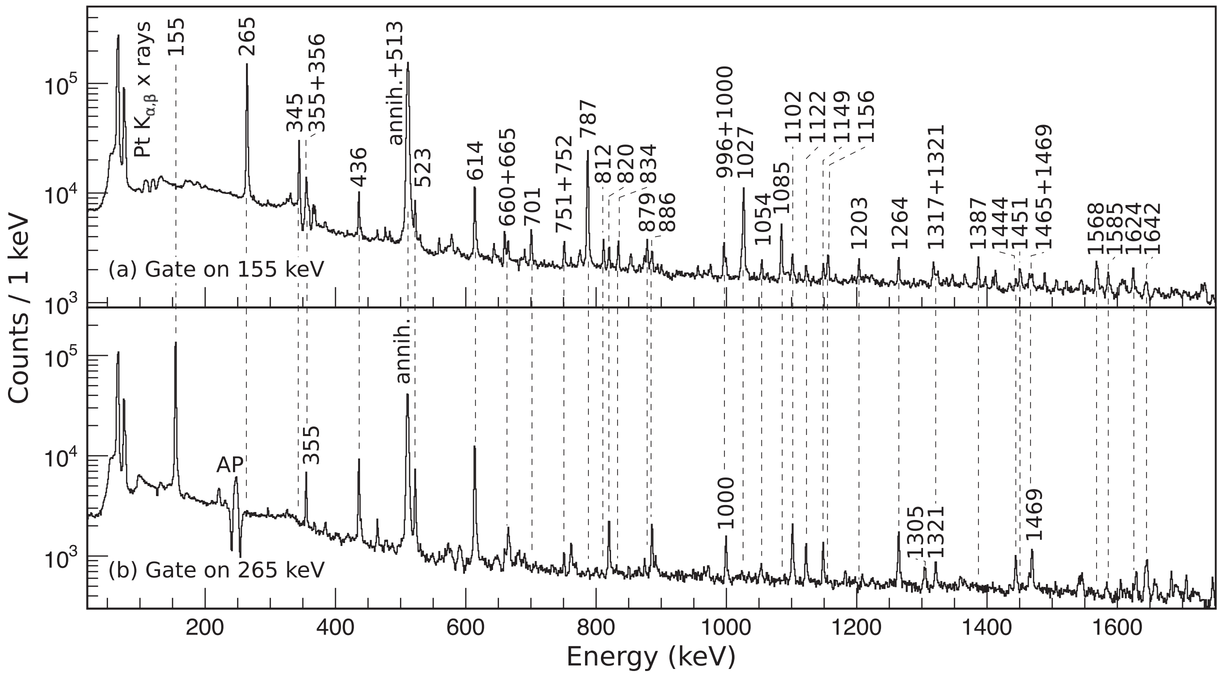

FIG. 2. Low-energy part of coincidence γ-ray spectra with the gate on (a) the 155-keV $2_1^+ \rightarrow 0_1^+$ transition, (b) the 265-keV $4_1^+ \rightarrow 2_1^+$ transition. AP denotes the artificial peak from Compton scattering.

B. Half-life of ^{182}Au

To determine the half-life of ^{182}Au, a measurement was done with no tape movement at the end of the implantation. Several decay curves were constructed by gating on the most intense γ-ray transitions in ^{182}Pt. Background subtraction was performed in the same way as for γ-γ coincidence spectra. An exponential function plus a constant background was used to fit the time distributions. An example of the decay curve obtained by gating on the 155-keV peak is shown in Fig. 4. A value of $T_{1/2} = 16.39(14)$ s was obtained for this transition. The weighted average of

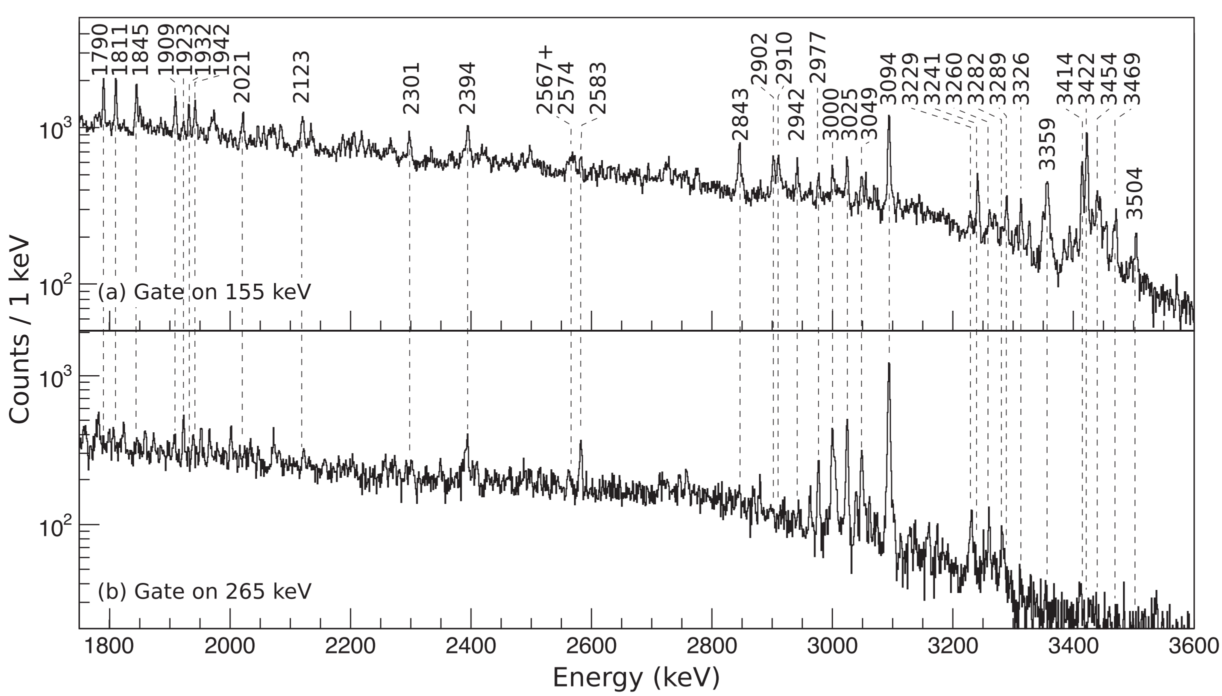

FIG. 3. High-energy part of coincidence γ-ray spectra with the gate on (a) the 155-keV $2_1^+ \rightarrow 0_1^+$ transition and (b) the 265-keV $4_1^+ \rightarrow 2_1^+$ transition.

TABLE I. A partial list of levels and transitions following the EC/β^+ decay of ^{182}Au. E_i and E_f are the respective energies of the initial and final states of the γ-ray transition with the energy E_γ. Values of the initial and final spin and parity I_i^π, I_f^π are taken from Refs. [22,36] or deduced from the analysis of deexcitation paths (see Sec. III C 1). Tentative transitions and levels are written in italics. Relative γ-ray intensities I_γ are normalized to the intensity of the 154.9-keV transition. Values determined from γ-γ coincidences are indicated with an asterisk. For the absolute intensity per 100 decays, multiply by 0.438(9). The full table is in Supplemental Material [40].

E_i (keV)	I_i^π	E_f (keV)	I_f^π	E_γ (keV)	I_γ
154.9(2)	2_1^+	0	0_1^+	154.9(2)	100
419.5(3)	4_1^+	154.9(2)	2_1^+	264.6(2)	45.7(19)
499.5(3)	0_2^+	154.9(2)	2_1^+	344.6(2)	7.44(32)
		0	0_1^+	499.5(3)[a]	3.82(43)
667.5(2)	2_2^+	154.9(2)	2_1^+	512.5(2)	28.2(35)*
		0	0_1^+	667.5(2)	9.64(41)
774.8(3)	6_1^+	419.5(3)	4_1^+	355.3(2)	1.18(16)*
855.6(1)	2_3^+	499.5(3)	0_2^+	356.1(2)	1.63(23)*
		419.5(3)	4_1^+	436.1(2)	2.98(13)
		154.9(2)	2_1^+	700.8(2)	1.18(16)*
		0	0_1^+	855.6(2)	17.20(73)
942.2(2)	(3_1^+)	667.5(2)	2_2^+	274.8(2)	0.47(10)*
		419.5(3)	4_1^+	522.6(2)	1.96(26)*
		154.9(2)	2_1^+	787.2(2)	16.68(65)
1033.5(2)	(4_2^+)	667.5(2)	2_2^+	366.0(2)	1.43(19)*
		419.5(3)	4_1^+	614.0(2)	5.72(24)
		154.9(2)	2_1^+	878.5(2)	0.90(12)*
1151.2(2)	(0_3)	667.5(2)	2_2^+	483.6(2)	0.48(8)*
		154.9(2)	2_1^+	996.3(2)	1.38(19)*
1181.4(1)	(2_4)	855.6(1)	2_3^+	325.9(2)	0.92(13)*
		499.5(3)	0_2^+	681.8(2)	0.09(3)*
		419.5(3)	4_1^+	761.8(2)	0.37(6)*
		154.9(2)	2_1^+	1026.5(2)	8.08(34)
		0	0_1^+	*1181.4(2)*	0.45(5)
1239.5(1)	4_3^+	942.1(1)	(3_1^+)	297.3(2)	0.14(3)*
		855.6(1)	2_3^+	383.9(2)	0.98(14)*
		774.8(3)	6_1^+	464.7(2)	0.37(6)*
		667.5(2)	2_2^+	572.6(5)	0.35(11)*
		419.5(3)	4_1^+	820.0(2)	0.95(4)
		154.9(2)	2_1^+	1084.6(2)	3.34(14)

[a]Observed only in the spectrum of conversion electrons.

half-life values from several intense γ-ray transitions shown in Table III in the Supplemental Material [40] is $T_{1/2} = 16.43(12)$ s. This value is more precise than the literature value of $T_{1/2} = 15.5(4)$ s [32] and agrees with it within 2σ. The same half-life for all measured transitions confirms that only a single state in the parent ^{182}Au was observed in our study.

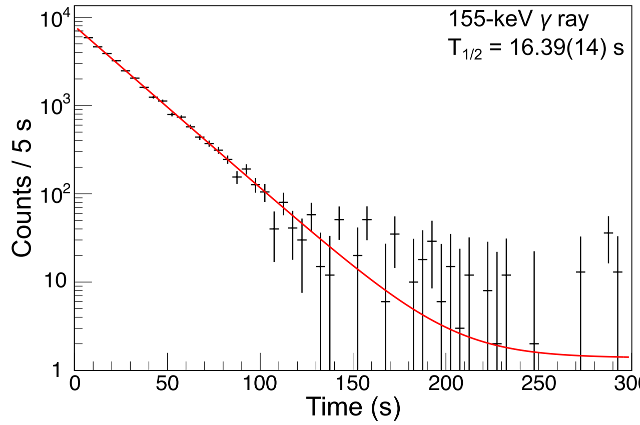

FIG. 4. Time distribution of the 155-keV transition. A sum of an exponential function and a constant background (red line) was used in the fitting procedure.

C. β decay of ^{182}Au

1. γ-ray analysis

In total, we identified 147 excited levels and 386 transitions in ^{182}Pt, of which 125 levels and 336 transitions are new. A summary of deduced levels and observed transitions with their relative intensities is in Table I. Figures 5 and 6 show the lowest parts of the deduced level scheme.

Almost all γ-ray transitions and all excited states reported in Ref. [36] were confirmed. The only exception is the 644-keV transition, which was tentatively placed between the 1419- and 775-keV levels in Ref. [36]. Based on γ-γ coincidences shown in Fig. 7, we placed the 644-keV transition between the 1311- and the 668-keV levels in the level scheme, see Fig. 5. If the previous placement was correct, then the 355-keV transition would be in coincidence with the 644-keV γ ray, but such coincidence was not observed, see Fig. 7.

We also confirm two tentative 1310.9- and 274.8-keV transitions deexciting the 1311- and 942-keV levels, respectively, reported in Ref. [28]. Five more lines reported as unplaced from this study with energies of 296.4, 865.3, 900.4, 1054.4, and 1203.5 keV were observed and placed in the level scheme, see Fig. 5.

The 6^+ 1863.4- and 5^- 1670.7-keV levels (see Fig. 4 in Supplemental Material [40] and Fig. 6, respectively), previously identified in the in-beam study [22], were also observed and placed into the β-decay scheme. This includes the 1444.0- and 1088.1-keV transitions deexciting the former and the 431.2-keV transition depopulating the latter level.

Three tentative γ-ray transitions connecting excited states directly to the g.s. with energies of 1181.4, 1568.0, and 1753.2 keV were identified as doublets. The intensities of these transitions were determined as the differences in the intensities from the singles γ rays and the intensities of their doublet counterparts obtained from the γ-γ coincidences. The energies of these transitions could not be determined directly, and therefore we consider them to be the same as the respective level energies, see Figs. 5 and 6 and Fig. 4 in Supplemental Material [40].

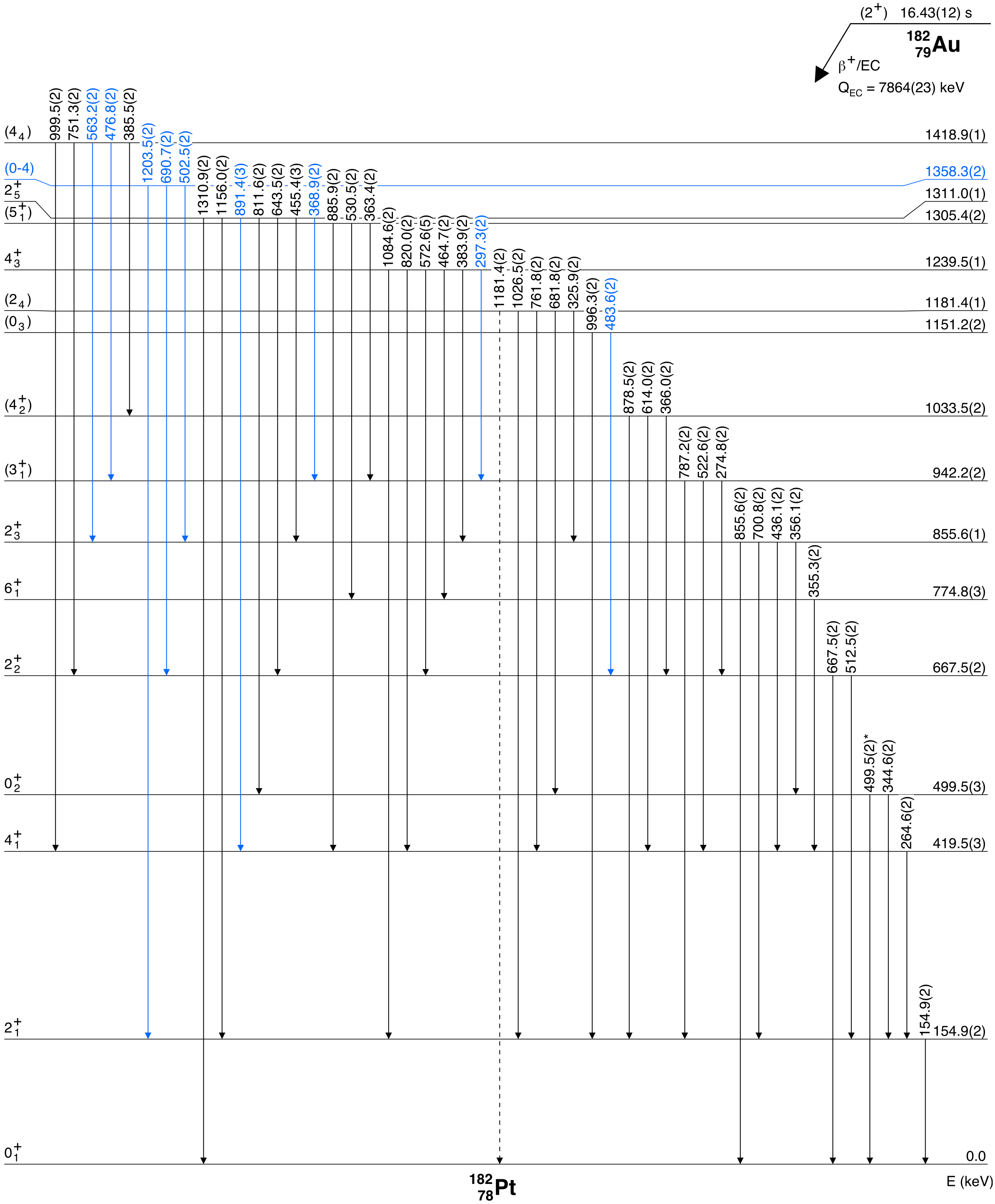

FIG. 5. Partial level scheme of excited states in ^{182}Pt populated in EC/β^+ decay of ^{182}Au, part 1/9. Transitions and levels highlighted in blue are newly observed. The spin and parity values are taken from Refs. [36] or deduced from the deexcitation paths. The 500-keV transition marked with an asterisk was observed only in the spectrum of conversion electrons. The dashed line represents a tentative transition. The whole level scheme is shown in Figs. 2–10 in the Supplemental Material [40].

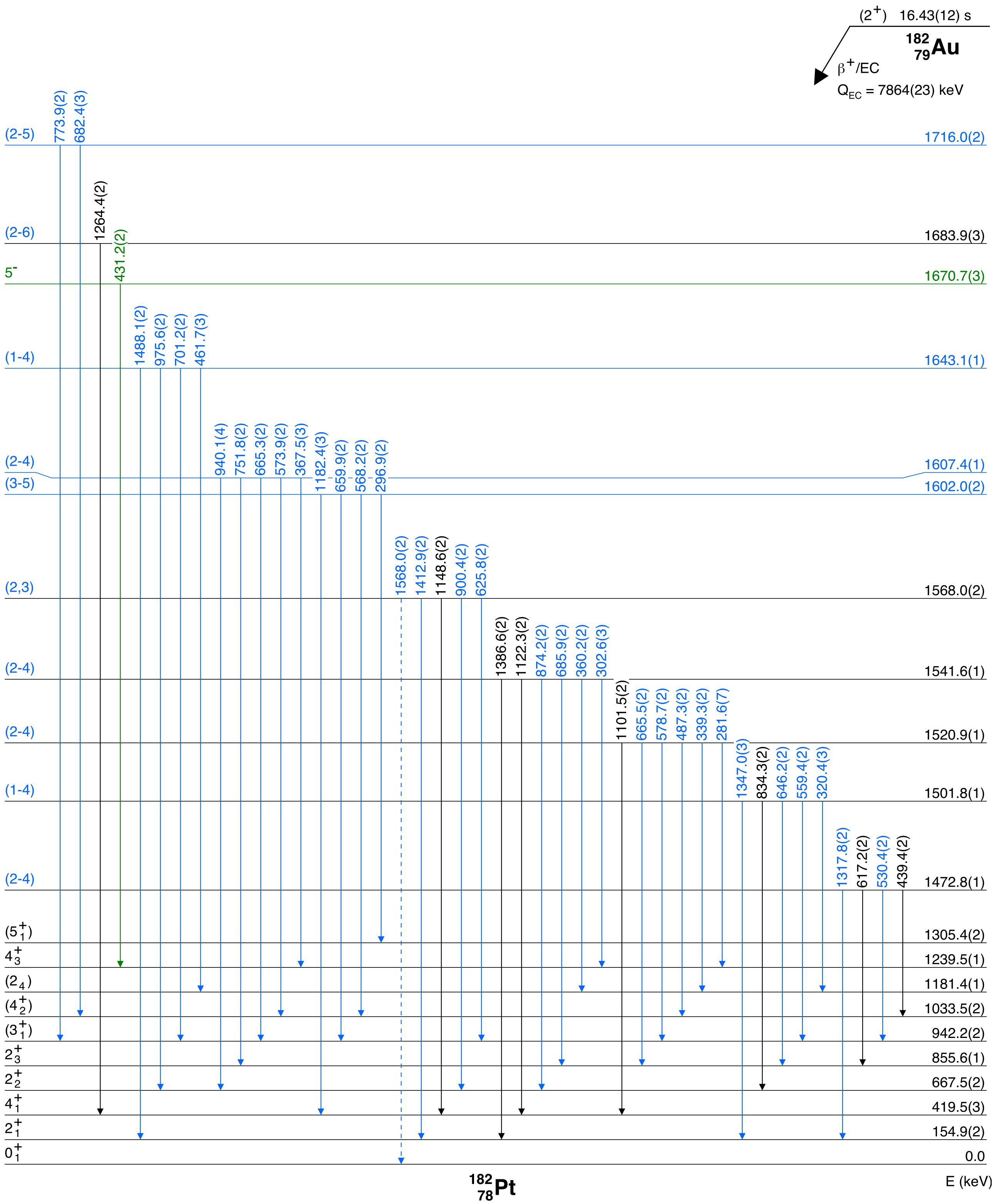

FIG. 6. Partial level scheme of excited states in ^{182}Pt populated in EC/β^+ decay of ^{182}Au, part 2/9. Transitions and levels highlighted in blue are newly observed, and the ones in green are known from the in-beam study [22]. The spin and parity values are taken from Refs. [22,36] or deduced from the deexcitation paths. The dashed line represents a tentative transition. The whole level scheme is shown in Figs. 2–10 in the Supplemental Material [40].

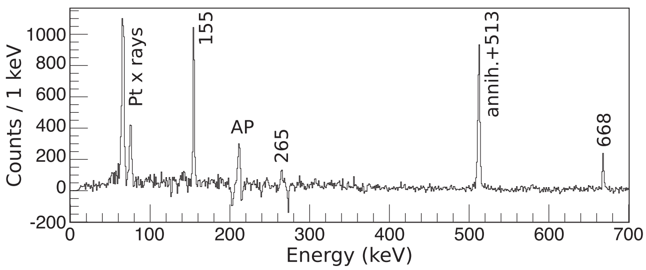

FIG. 7. Background-subtracted γ-rays in coincidence with the 643.5-keV transition. A small peak at 265 keV is caused by the presence of the 646-keV transition in the gated region. AP denotes the artificial peak caused by Compton scattering.

Because of the prompt character of γ rays observed in ^{182}Pt, we only consider the $E1, M1, E2$, or $M2$ multipolarities for transition energies below 1.3 MeV, and we also include $E3$ for higher energies. This allows us to tentatively establish $I = (2, 3)$ for levels at 1568.0, 2005.7, and 2075.8 keV and $I = (1, 2)$ for 1721.9-, 1753.2-, and 1965.5-keV states. Similarly, spins of other levels were tentatively restricted to specific ranges based on the connecting transitions to levels with known I^{π}, see Table I in the Supplemental Material [40].

The intensity of the 513-keV transition (see Fig. 5) could not be determined directly from the singles γ rays (Fig. 1) or the coincidence spectra because of its vicinity to the annihilation peak at 511 keV. All transitions feeding the 668-keV state deexcite via the 668-keV γ rays or the 513-155-keV cascade. We compared the intensity of these transitions in coincidences gated on the 155- and the 668-keV transitions. This resulted in the intensity ratio for the 513- and 668-keV γ rays and, subsequently, the intensity of the 513-keV line.

2. Conversion electron analysis

The conversion electron spectrum shown in Fig. 8 was analyzed to search for $E0$ transitions. The intensity of the 499.5 keV ($0^+_2 \rightarrow 0^+_1$) $E0$ transition, necessary for the β-decay feeding determination (Sec. III D), was obtained from the number of detected K electrons after correction for the CE detection efficiency of the silicon detectors (see Table I). Other shells were accounted for by the theoretical fraction of K conversion from the BrIcc [46].

For the 455-keV transition ($2^+_5 \rightarrow 2^+_3$), only conversion electrons were observed in previous studies [28,36] with no corresponding γ rays. Thus, $E0$ multipolarity was assumed for this transition and lower limits on K internal conversion coefficient (ICC) were reported (see Table II). We observed K conversion electrons from this transition together with a weak γ-ray transition of the corresponding energy, and therefore a mixed $E0 + M1 + E2$ multipolarity can be attributed to the 455.4-keV transition. The resulting ICC α_K is much higher than the theoretical value for the $M1$ multipolarity, pointing to a strong $E0$ component, confirming the previous suggestion.

We determined ICCs for two other transitions, the 513-keV $2^+_2 \rightarrow 2^+_1$, and the 701-keV $2^+_3 \rightarrow 2^+_1$, which are summarised together with previous values in Table II. An $E0$ component has been attributed to both transitions. Previously reported values of K ICCs for the 513-keV γ ray are mutually exclusive (>0.165 [28] and 0.044(6) [36]), and our value $\alpha_K = 0.055(7)$ agrees within uncertainty with the latter one. Good agreement is also obtained with the value $\alpha_K^{\mathrm{ref}}(513) = 0.062(13)$ from the ENSDF evaluation [47], where the CE intensity from Ref. [28] and γ-ray intensity from Ref. [36] were combined. The existence of the $E0$ component of the 513-keV transition has already been questioned in Ref. [36] because of the measured ICC being smaller than the theoretical value for the $M1$ multipolarity. Our values are larger but consistent within uncertainties with the theoretical values, see Table II, for both the K and L conversion. Because of this, we cannot confirm the presence of the $E0$ component in this transition. This is in agreement with the 486-keV $2^+_2 \rightarrow 2^+_1$ transition in ^{184}Pt, where also no $E0$ component could be reliably assigned [48].

In the case of the 701-keV transition, our conversion coefficient $\alpha_K = 0.78(13)$ agrees with both reported values (0.73(22) [28] and >0.27 [36]) within uncertainty. Its value is much larger than the theoretical ICC for the $M1$ multipolarity, confirming the $E0$ component of this transition. Previously reported mixing ratio $\delta(E2/M1, 701) = 0.7^{+1.0}_{-0.3}$ [36] allows us to extract the $q^2_K(E0/E2)$ mixing ratio for this transition. Using the following equation [49]:

$$q^2_K = \frac{\alpha_K^{\mathrm{exp}}(1+\delta^2) - \alpha_K(M2)}{\delta^2 \alpha_K(E2)} - 1, \qquad (1)$$

where $\alpha_K(M1)$ and $\alpha_K(E2)$ are theoretical ICCs taken from the BrIcc [46], we obtained the value of $q^2_K = 258^{+460}_{-160}$. Such a high q^2_K value indicates a mixing between two coexisting bands of different deformation built on top of the 0^+_1 and 0^+_2 states, as was suggested in Ref. [36].

TABLE II. Experimental internal conversion coefficients α_{exp} of transitions in ^{182}Pt for given atomic shells compared with previously published values α_{ref} from Refs. [28,36] and theoretical values α_{th} calculated using BrIcc [46].

E (keV)	E_i (keV)	E_f (keV)	$J_i \rightarrow J_f$	Shell	α_{exp}	α_{ref} [28]	α_{ref} [36]	$\alpha_{\mathrm{th}}(M1)$ [46]	$\alpha_{\mathrm{th}}(E2)$ [46]
455.4(3)	1311.0(1)	855.6(1)	$2^+_5 \rightarrow 2^+_3$	K	14.8(65)	>1.7	>0.32	0.0824(12)	0.0225(4)
512.5(3)	667.5(3)	154.9(2)	$2^+_2 \rightarrow 2^+_1$	K	0.055(7)	>0.165[a]	0.044(6)[a]	0.0604(9)	0.0173(3)
				L	0.010(3)			0.00972(4)	0.00458(7)
700.8(2)	855.6(1)	154.9(2)	$2^+_3 \rightarrow 2^+_1$	K	0.78(13)	0.73(22)	>0.27	0.0269(4)	0.00892(13)

[a]The value of $\alpha_K = 0.062(13)$ was obtained in the ENSDF [47] evaluation combining the CE intensity from Ref. [28] and γ-ray intensity from Ref. [36].

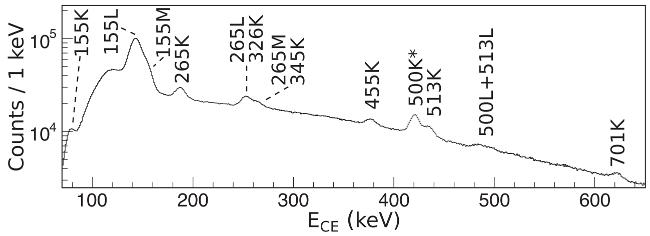

FIG. 8. Conversion electrons measured by the silicon PIN array. Peaks are marked with transition energy and the corresponding atomic orbital. The 500-keV transition observed only in the spectrum of conversion electrons is marked with an asterisk.

D. β-decay feeding intensities

Total transition intensities were calculated using internal conversion coefficients from this work, or they were taken from BrIcc [46], see Table I in the Supplemental Material [40]. As was previously mentioned, prompt character of γ-ray transitions limits their multipolarity to $E1$, $M1$, $E2$, $M2$, or $E3$ for higher energies. For transitions with unknown multipolarity, average values of ICCs for $E1$ ($\alpha_{\mathrm{tot},E1}$) and $M2$ ($\alpha_{\mathrm{tot},M2}$) multipolarity were used as they are the smallest and the largest among the considered ICCs, respectively. The uncertainty of the average value was calculated as half of the difference between these two ICCs to cover the whole range of possible values.

Table III contains values of β-decay feeding intensities to excited states in ^{182}Pt calculated from the balance of total transition intensities feeding and depopulating each level. The relative feeding of each state was normalized to the total number of ^{182}Au β decays. It was calculated as the sum of all γ-ray transitions deexciting directly to the g.s., giving the total intensity of the 155-keV transition of 43.8(9) per 100 β decays. The intensity values were corrected for the β-decay branching ratio of ^{182}Au $b_\beta = 99.871(11)\%$ determined in this work, see Sec. III E 2. The direct feeding of the $I^\pi = 0^+$ g.s. of ^{182}Pt by the β decay of the $I^\pi = (2^+)$ g.s. of ^{182}Au [6] is considered to be negligible, because it would be the second forbidden nonunique β decay [50]. The NNDC log ft calculator [51] was employed to calculate the log ft values using $Q_{\mathrm{EC}}(^{182}\mathrm{Au}) = 7864(23)$ keV [52], half-life of 16.43(12) s and β-decay feeding intensities from this work. Fermi integrals for the allowed and first forbidden nonunique decays (f_0), as well as for the first forbidden unique decays (f_1) were used. Corresponding log f_0t and log f_1t values are in Table III.

Values of β-decay feeding intensity are often artificially increased by the unobserved γ-ray feeding from the higher-lying excited states, the so-called pandemonium effect [53], especially in the case of relatively low-lying levels and high total Q_β value. Therefore, the β-decay feeding intensities and log ft values in Table III should be considered as the upper and lower limits, respectively. The direct evidence for the pandemonium effect from our data will be discussed in Sec. IV A.

TABLE III. Values of β-decay feeding intensities I_β into excited levels of ^{182}Pt and corresponding log ft values for allowed and the first forbidden nonunique decay (log f_0t) and for the first forbidden unique decay (log f_1t). The values of spin and parity are taken from Refs. [22,36] or deduced from the analysis of deexcitation paths (marked with an asterisk). The full table is in the Supplemental Material [40].

E (keV)	I^π	I_β (%)	log f_0t	log f_1t
154.9(2)	2_1^+	10.9(21)	6.09(10)	8.18(10)
419.5(3)	4_1^+	7.2(10)	6.19(7)	8.25(7)
499.5(3)	0_2^+	1.58(30)	6.84(10)	8.89(10)
667.5(2)	2_2^+	8.9(16)	6.04(9)	8.08(9)
774.8(3)	6_1^+	0.22(8)	7.61(20)	9.64(20)
855.6(1)	2_3^+	4.63(52)	6.27(6)	8.29(6)
942.2(2)	(3_1^+)	4.21(40)	6.29(4)	8.30(4)
1033.5(2)	(4_2^+)	2.03(20)	6.56(4)	8.56(4)
1151.2(2)	(0_3)	0.61(10)	7.07(8)	9.06(8)
1181.4(1)	(2_4)	3.06(26)	6.36(4)	8.35(4)
1239.5(1)	4_3^+	1.80(15)	6.57(4)	8.55(4)
1305.4(2)	(5_1^+)	0.37(6)	7.24(8)	9.21(8)
1311.0(1)	2_5^+	2.88(20)	6.35(3)	8.32(3)
1358.3(2)	(0-4)*	0.25(7)	7.40(14)	9.37(14)

E. α decay of ^{182}Au

1. α-γ coincidence analysis

Three fine structure α decays of ^{182}Au were reported in the previous study [30] at 5283(5), 5352(5), and 5403(5) keV, with the latter being assigned to feed the ^{178}Ir g.s. A 55-keV γ ray was also reported in coincidence with the 5352-keV decay, see Table IV. All these decays are visible in the singles α-decay spectrum of ^{182}Au in Fig. 9(a). An α-γ coincidence spectrum in Fig. 9(b) was constructed using the time window of 200 ns and four groups of α-γ coincidences were identified at 5350(5)-55 keV, 5293(8)-115 keV, 5282(5)-128 keV, and 5282(5)-84 keV. The first of them and the strongest one is the only α-γ coincidence reported in Ref. [30]. The second one is in a good agreement with the $Q_{\alpha,\mathrm{tot}}(5402) = 5524(5)$ keV, establishing a new excited level at 114.7(5) keV in ^{178}Ir. The third group also agrees with $Q_{\alpha,\mathrm{tot}}(5402)$, and, thus, the observed 127.5(7) keV γ ray gives the more precise energy for the previously reported 123(7)-keV state; see the α-decay scheme of ^{182}Au in Fig. 10.

The 5282-84 keV group indicates that the 128-keV level also deexcites by the 84-keV transition. We note that a γ-ray transition of similar energy was reported in Ref. [54] but not placed in the level scheme. Since this transition does not match the energy differences between the established levels, we cannot place it reliably in the decay scheme.

Besides the dominant 55-keV transition, a small peak at 46 keV is visible in α-γ coincidences gated on the 5350-keV peak [see Fig. 11(a)]. Its energy matches the energy of the Compton backscatter peak for the 55-keV γ ray, therefore, we do not consider it to be a real transition.

The coincidence spectrum for the 5282- and 5293-keV α decays [Fig. 11(b)] shows the 128-, 115- and 84-keV transitions and iridium $K_{\alpha,\beta}$ x rays. While the energy of K_α matches

TABLE IV. A summary of observed α-γ coincidences for the α decay of ^{182}Au in this work and the previous study [30]. Tentative transitions are given in italics. Reduced α-decay widths δ_α^2 were obtained using the Rasmussen approach [56]. Hindrance factors HF were extracted relative to the weighted average value of $\delta_\alpha^2 = 64(13)$ keV for the unhindered α decays in ^{181,183}Au [30,57,58].

This work						Previous results [30]			
E_α (keV)	E_γ (keV)	$Q_{\alpha,\mathrm{tot}}$ (keV)	I_α (%)	δ_α^2 (keV)	HF	E_α (keV)	E_γ (keV)	I_α (%)	HF
5402(5)	–	5524(5)	15.6(4)	2.4(3)	26(6)	5403(5)	–	21	21
5350(5)	55.0(2)	5525(5)	75.7(10)	21(2)	3.0(7)	5352(5)	55.4	72	3
5293(8)	114.7(5)	5527(9)	0.7(6)	0.4(3)	175(163)				
5282(5)	127.5(7), 83.8(6), *76.3(12)*	5529(5)	7.4(7)	4.6(6)	14(4)	5283(5)	–	7	28
5185(6)	–	–	0.63(7)	1.2(2)	52(13)				

the tabulated value, the K_β peak is shifted (75.3(5) keV, $E(\mathrm{Ir}\ K_\beta) = 73.8$ keV [55]) and wider compared to other γ-ray peaks. Because of this, we consider it as a doublet of the iridium K_β x ray and a tentative 76-keV transition. We do not place this transition in the level scheme.

An additional 5185(6)-keV α-decay peak is visible in the singles α spectrum [Fig. 9(a)]. No γ rays were observed in coincidence, but a group of iridium K_α x rays is present in Fig. 9(b). We assign this decay as a new tentative fine structure component of ^{182}Au α decay feeding a 223-keV level.

A summary of observed α decays and coincident γ rays is in Table IV. The intensities of fine structure α decays were taken from the singles spectrum [Fig. 9(a)]. The intensity of the combined 5282- and 5293-keV peak was divided based on α-γ coincidence counts of the 115-keV and 128-, 84-, and 76-keV γ-rays corrected for the γ-ray detection efficiency and internal conversion. The average values of ICCs for $E1$ and $M1$ ($E2$ for the 76 keV) multipolarity from Ref. [46] were used in the same way as for ^{182}Au β decay (see Sec. III D). Potential coincidence summing of α particles and CEs was investigated using a GEANT4 simulation and was found to be negligible.

Reduced α-decay widths δ_α^2 were calculated using the Rasmussen approach [56] assuming $\Delta L = 0$ decays. We will discuss the α-decay branching ratio $b_\alpha(^{182}\mathrm{Au})$ used in the calculation separately in Sec. III E 2. Hindrance factors HF were calculated relative to the average δ_α^2 value of the unhindered α decays in neighboring ^{181}Au ($3/2^- \rightarrow 3/2^-$) and ^{183}Au ($5/2^- \rightarrow 5/2^-$) calculated from published data [30,57,58] [75(16) and 45(21), respectively].

We obtained the low hindrance factor of 3.0(7) for the 5352-keV α decay, which agrees with the previously published value of HF = 3 [30]. This supports conclusion on the same structure of the 55-keV level and the ^{182}Au g.s. given

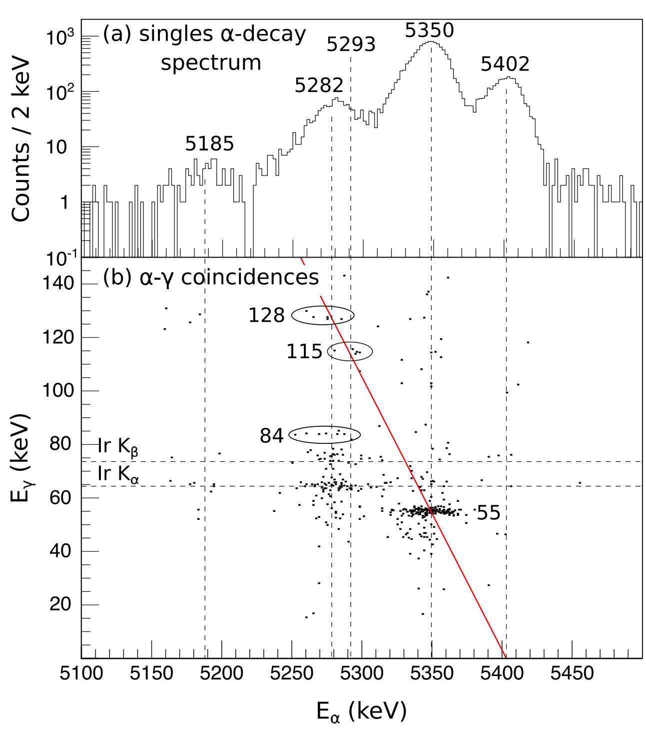

FIG. 9. (a) Singles α-decay spectrum of ^{182}Au. (b) α-γ coincidences for ^{182}Au. The red line denotes $Q_{\alpha,\mathrm{tot}} = Q_\alpha + E_\gamma = 5524$ keV determined from the 5350-55-keV coincidence.

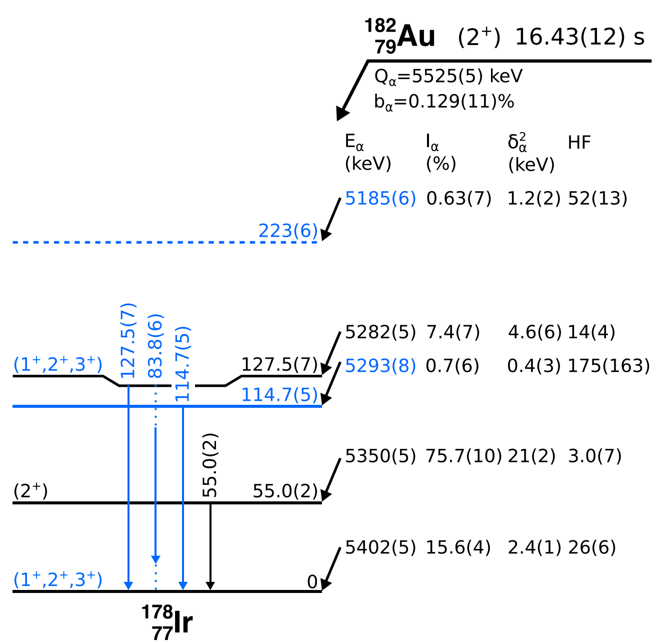

FIG. 10. α-decay scheme of ^{182}Au. Tentative transitions and levels are given with dashed lines. New levels and transitions are highlighted in blue.

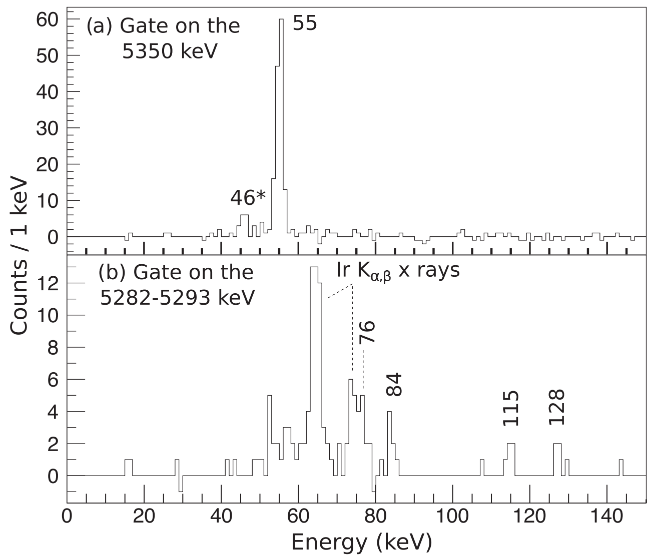

FIG. 11. Spectra of γ rays in coincidence with (a) the 5350-keV and (b) the 5282- and 5293-keV α transitions. A peak at 46 keV marked with an asterisk is not considered to be a real transition; see the text for details.

in Ref. [30]. Therefore, a $I^\pi = (2^+)$ can be attributed to the 55-keV state based on the (2^+) assignment for ^{182}Au [6].

The internal conversion coefficient of the 55-keV γ-ray $\alpha_{\text{tot}}(55) = 11.7(12)$ was obtained by comparing the number of γ-efficiency corrected number of coincident pairs [see Fig. 11(a)] and α counts of the 5350-keV line in the singles spectrum. It lies between the theoretical values for $M1$ and $E2$ multipolarities (6.16 and 67.02, respectively [46]), therefore, we assign it the mixed $M1 + E2$ multipolarity. This gives an $I^\pi = (1^+, 2^+, 3^+)$ for the ^{178}Ir g.s.

The hindrance factor of the 5282-keV decay is lower than for the 5402-keV decay to the g.s. in ^{178}Ir [14(4) compared to 26(6)]. We can expect a similar or smaller change in nuclear structure for the decay to the 128-keV level, therefore, we assigned to it the same $I^\pi = (1^+, 2^+, 3^+)$.

2. ^{182}Au α-decay branching ratio

The α-decay branching ratio of ^{182}Au was calculated in two ways. The first method used the number of α and β decays of this isotope:

$$b_\alpha(^{182}\text{Au}) = \frac{N_\alpha(^{182}\text{Au})}{N_\alpha(^{182}\text{Au}) + N_\beta(^{182}\text{Au})}. \qquad (2)$$

The number of β decays of ^{182}Au was deduced indirectly via the 155-keV γ ray in ^{182}Pt, see Sec. III A. Note that the branching ratio calculated in this way is influenced by the pandemonium effect, making it an upper limit.

The second method compared the α-decay counts of both ^{182}Au and ^{182}Pt:

$$b_\alpha(^{182}\text{Au}) = \frac{N_\alpha(^{182}\text{Au})}{N_\alpha(^{182}\text{Au}) + \frac{N_\alpha(^{182}\text{Pt})}{b_\alpha(^{182}\text{Pt})}}, \qquad (3)$$

where $b_\alpha(^{182}\text{Pt})$ is the α-decay branching ratio of ^{182}Pt. Two values were reported in previous studies, $b_\alpha(^{182}\text{Pt}) = 0.023^{+0.023}_{-0.012}\%$ [59] and $b_\alpha(^{182}\text{Pt}) = 0.038(2)\%$ [30], of which we used the latter, more precise value in our calculation. Only decay periods of the measured data without tape movement were used. These periods were not long enough for all ^{182}Pt nuclei to decay ($\approx$4 ^{182}Pt half-lives), therefore, a correction accounting for the unobserved decays was applied.

The resulting branching ratios obtained using both methods are $b_\alpha(^{182}\text{Au}) = 0.117(13)\%$ and $b_\alpha(^{182}\text{Au}) = 0.129(11)\%$, respectively. Both agree with each other within uncertainty and with the previously reported value of $b_\alpha(^{182}\text{Au}) = 0.13(5)\%$ [30]. Since the first value is affected by the pandemonium effect, the second value $b_\alpha(^{182}\text{Au}) = 0.129(11)\%$ [corresponding to $b_\beta(^{182}\text{Au}) = 99.871(11)\%$] has been used for the calculation of β-decay feeding intensities to excited levels in ^{182}Pt.

IV. DISCUSSION

A. β-decay feeding intensities

The dominant β-decay feeding in this study was observed to several 2^+ states (e.g., the 2^+_1 and 2^+_2 states at 155 and 668 keV), as can be seen in Table III. The 942-keV (3^+_1) state was also strongly fed. This pattern is expected for the β decay of the $I^\pi = (2^+)$ g.s. in ^{182}Au [6]. A surprisingly high β-decay feeding to 4^+ states is also seen, especially for the 4^+_1 level at 420 keV ($I_\beta = 7.3\%$). The latter is not consistent with the decay of the $I^\pi = (2^+)$ parent state. The $\log f_0t$ values for the population of all $I = 2$–4 states are in the range of 6.0–6.6 (see Table III), which is in line with the allowed or the first forbidden nonunique decays. Moreover, $\log f_1t$ values for these decays are below or comparable to the recommended lower limit for the first forbidden unique decay $\log f_1t \geqslant 8.5$ [50]. However, this is in strong disagreement in the case of 4^+ states, as it would lead to the second forbidden nonunique β decay with recommended lower limit of $\log f_1t \gtrsim 11$ [50]. Possible explanations will be discussed further, namely the 3^+ assignment for the g.s. of ^{182}Au, a new isomeric state in ^{182}Au, and the pandemonium effect.

1. A scenario of I = 3 for ^{182}Au g.s.

The natural explanation of the comparable β-decay feeding to the 2^+ and 4^+ levels would be the $I^\pi = 3^+$ for the g.s. of ^{182}Au. The first determination of ^{182}Au g.s. spin was performed in a low-temperature orientation study at ISOLDE [33]. A range of spins $I = 2$–4 was proposed, with $I = 3$ being the preferred value. However, later ^{182}Hg β-decay study rejected $I = 3, 4$ because of the observed $M1$ transitions connecting 1^+ states directly to the ^{182}Au g.s. and proposed $I^\pi = (2^+)$ [34]. The same assignment was also proposed in the laser-spectroscopy measurement at ISOLDE [6]. The recent experiment at CRIS with better laser resolution also suggested the $I^\pi = (2^+)$ assignment [60], therefore, the $I^\pi = 3^+$ option can be excluded.

2. A scenario of $I = 5$ isomer in ^{182}Au

The second possible cause of this substantial feeding of the 4^+ states is the presence of another β-decaying state in ^{182}Au preferentially feeding those levels. In the following discussion, we consider only states living long enough ($\gtrsim$100 ms) to be delivered to and detected at IDS. The only possibility is $I \geqslant 5$ since other states would not be isomeric with sufficiently long half-life alongside the 2^+ g.s. of ^{182}Au or would lead to highly suppressed β decays to 4^+ states [50]. We note that in the recent NUBASE evaluation [35], a 5^- isomer was proposed for this isotope because of the direct feeding of the 4^+ and 5^+ states evaluated based on γ-ray intensities from Ref. [36]. Two β-decaying states are known in the ^{184}Au, 5^+ g.s. and 2^+ excited state at 68.5 keV. The configuration of this 2^+ state is the same as for the (2^+) g.s. in ^{182}Au, $\pi 3/2^-[532]h_{9/2} \otimes \nu 1/2^-[521]p_{3/2}$ [4,6].

To investigate the low-lying one-proton one-neutron quasiparticle excitations in ^{182}Au, we have also conducted configuration-constrained potential energy surface (CCPES) calculations [61] employing a nonaxially deformed Woods-Saxon potential [62] with the "universal" parametrization [63]. The total energy incorporates a macroscopic part derived from the liquid-drop model [64] and a microscopic component accounting for Strutinsky shell corrections [65] and pairing correlations. To avoid the possible pairing collapse in multiquasiparticle systems, we implemented the Lipkin-Nogami (LN) approximation [66] to estimate particle-number projection. The monopole pairing strength G was determined through the average gap method [67].

For multiquasiparticle configurations, the microscopic energy explicitly includes contributions from unpaired particles occupying the single-particle orbits specified by the given configuration. Configuration-dependent blocking effects were rigorously treated by excluding the singly occupied orbitals from the LN calculation. The CCPES computations were executed across a three-dimensional deformation lattice spanning $(\beta_2, \gamma, \beta_4)$ parameters. The resulting potential energy surfaces enable self-consistent determination of nuclear deformation characteristics, excitation energies, and pairing interaction properties for multiquasiparticle states.

Experimental and theoretical excited states in ^{182}Au are compared in Fig. 12. Calculations predict $I^\pi = 2^+$ g.s. with the same configuration as was deduced in Ref. [6]. The lowest excited states are also reproduced to some degree. The calculations also show a 5^+ excited state in ^{182}Au at $E = 135$ keV with configuration $\pi 3/2^-[532] \otimes \nu 7/2^-[514]$, which is the same assignment as for g.s. in ^{184}Au [4]. This state was not observed in the β-decay study of ^{182}Hg [34] (see Fig. 12), which is expected for the decay of 0^+ g.s., but if it exists, it could be directly produced in our experiment. Rotational states are not included in the calculations, but $I = 3, 4$ members of the rotational band built on top of the $I = 2$ g.s. bandhead are expected to exist in ^{182}Au lie below the 5^+ level, considering the same moment of inertia as for the yrast band in ^{184}Au [68] thanks to similar deformation of these nuclei [9]. These levels would provide a deexcitation path for the 5^+ state, making it nonisomeric. The same calculations correctly reproduced the 5^+ g.s. in ^{184}Au, with a 2^+ excited, albeit not isomeric, state.

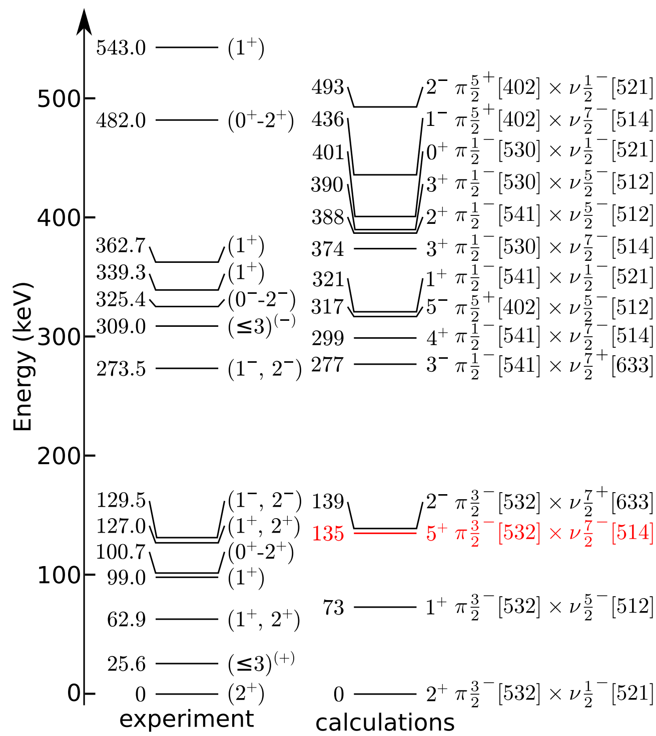

FIG. 12. Comparison of experimental [32,34] (left) and calculated excited levels (right) in ^{182}Au. The predicted 5^+ level is highlighted in red.

Moreover, in the case of $I = 5$ isomer, we would expect strong direct β-decay feeding also to the states with spins 5 and 6 in ^{182}Pt. As can be seen in Table III, β-decay feeding intensity to these states is much lower compared to the feeding of the 4^+ states, for example, 7.3(10)% and 0.22(8)% for the 4^+_1 and 6^+_1 levels, respectively. We can also compare the ratio of intensities $I_\gamma(6^+_1 \to 4^+_1)/I_\gamma(4^+_1 \to 2^+_1)$ for ^{182}Pt and ^{184}Pt where both the 2^+ and 5^+ long-lived states are feeding exciting levels. This ratio decreases from $\sim$1/2 in ^{184}Pt [69] to $\sim$1/40 in ^{182}Pt, showing that the β decay of the 5^+ g.s. in ^{184}Au results in much stronger direct or indirect feeding from higher-spin states to the 6^+_1 level.

Additionally, no hyperfine structure of the 267.6-nm transition corresponding to an additional long-lived state in ^{182}Au has been observed in laser spectroscopy measurement despite the use of a wide frequency range [70] (see Fig. 11 in Supplemental Material [40]). There might be a possibility that the isomer was missed in the laser spectroscopy study because of overlapping hyperfine components of the measured transition corresponding to the ground and isomeric states. However, such an exact overlap is unlikely, and a substantial contribution of such an isomer would also distort intensity ratios of hyperfine components attributed to the $I = 2$ g.s. (see Fig. 7(a) in Ref. [6]). Therefore, even if the isomer existed, its contribution would have to be small and could not explain the large apparent β-decay feeding to the 4^+_1 state. Additionally, half-life values obtained from different transitions in this work (see Table III in Supplemental Material [40]) are consistent with the decay of a single state, and no statistically significant deviations were observed. Because of the arguments above, we conclude that there is no evidence for the $I = 5$ isomeric state in ^{182}Au.

3. Pandemonium effect

The third considered explanation of the substantial apparent β-decay feeding of the 4^+ states in ^{182}Pt is the unobserved feeding from higher-lying levels because of the pandemonium effect [53]. While the two previous scenarios ($I = 3$ or $I = 5$ for the parent state in ^{182}Au) were ruled out, pandemonium effect influences most of high-resolution γ-ray spectroscopy measurements, and, therefore, we consider it to be the main source of aforementioned feeding. However, this is unexpected for the 4^+ states, since the β decay of the (2^+) ^{182}Au g.s. dominantly feeds the $I = 1$–3 states, which one could expect to deexcite mainly to the $I \leqslant 3$ levels. Although we were able to detect high-energy γ rays (see Fig. 3 or Fig. 1 in Supplemental Material [40]) and we expanded the level scheme of ^{182}Pt up to $\approx$3.7 MeV of excitation energy (see Table I) in comparison to 1.9 MeV from Ref. [36], there remains a high probability for the unobserved feeding because of the high $Q_{\rm EC}$ value of 7864(23) keV [52]. The scenario of pandemonium effect is also supported by the total absorption spectroscopy measurement of ^{182}Au, where direct β-decay feeding up to 6 MeV in the excitation energy was observed, see Fig. 3(b) in Ref. [71]. It needs to be noted that although no β-decay feeding below 3 MeV was reported in Ref. [71], the low-energy part of the spectrum should be regarded with caution, according to the authors. Therefore, we cannot draw conclusions based on this part of the spectrum.

In total, β-decay feeding intensity into newly observed states makes up about 45% of all feeding assigned in the present work. Table V compares β-decay feeding intensity from our work and values calculated from previously published γ-ray intensities. It can be seen that after expanding the decay scheme in our study, the feeding intensity of the 2_1^+ 155-keV state decreased to about a third of that from Ref. [36], while the feeding of the 4_1^+ 420-keV state decreased only slightly. This indicates that levels indirectly feeding the 4_1^+ state are relatively high-lying, outside of the scope of our level scheme extension.

B. Differences in feeding of bands in ^{182}Pt

A simplified decay scheme with only the main levels to highlight the most dominant features of β-decay feeding from ^{182}Au is shown in Fig. 13. The first three 2^+ states in ^{182}Pt (2_1^+ at 155 keV, 2_2^+ at 668 keV and 2_3^+ at 856 keV) were identified as members of three different band structures [22,28]. The yrast band is a deformed prolate band with $K = 0$, the second band has a weakly oblate shape with $K = 0$, and the third one is the γ band with $K = 2$. Since g.s. of ^{182}Au has $K = 2$, a certain hindrance in β decay to the levels with $K = 0$ could be expected. A recent review showed that $\Delta K = 2$, $\Delta J = 0$ decay can lead to log ft values in the range of 9–10 [72]. However, the systematics considered cases with low Q_β values and without mixing of levels in the daughter isotope. We observed comparable feeding intensities for the 2^+ levels resulting in roughly the same log ft values [6.09(10), 6.04(9), and 6.27(6) for the 2^+_{1-3}, respectively], indicating no K hindrance in these β decays. This is probably caused by the mixing between the three bands, which was discussed in detail in Ref. [36] and the large effective Q values $Q_{\beta,\rm eff} =$

TABLE V. Comparison of previously known values of β-decay feeding intensities $I_\beta^{\rm ref}$ calculated from published data [47] and those determined in this work I_β. Values of spin and parity I^π are taken from Ref. [36].

Level (keV)	I^π	$I_\beta^{\rm ref}$ (%)	I_β this work (%)
154.9	2_1^+	31(2)	10.9(21)
419.5	4_1^+	11.4(8)	7.2(10)
499.5	0_2^+	5.2(7)	1.58(30)
667.5	2_2^+	10(2)	8.9(16)
774.8	6_1^+	0.10(35)	0.22(8)
855.6	2_3^+	7.1(8)	4.63(52)
942.1	(3_1^+)	7.4(9)	4.21(40)
1033.5	(4_2^+)	4.9(11)	2.03(20)
1151.2	(0_3)	1.3(1)	0.61(10)
1181.4	(2_4)	4.9(5)	3.06(26)
1239.5	4_3^+	5.3(4)	1.80(15)
1305.4	(5_1^+)	1.0(3)	0.37(6)
1311.0	2_5^+	2.3(3)	2.88(20)
1418.9	(4_4)	1.8(4)	0.97(10)
1472.8		1.5(4)	1.54(11)
1501.8		1.8(4)	1.13(11)
1520.9		0.75(24)	0.74(11)
1541.6		0.79(20)	1.31(14)
1683.9		0.61(14)	0.45(6)
1888.7		0.47(14)	0.60(8)

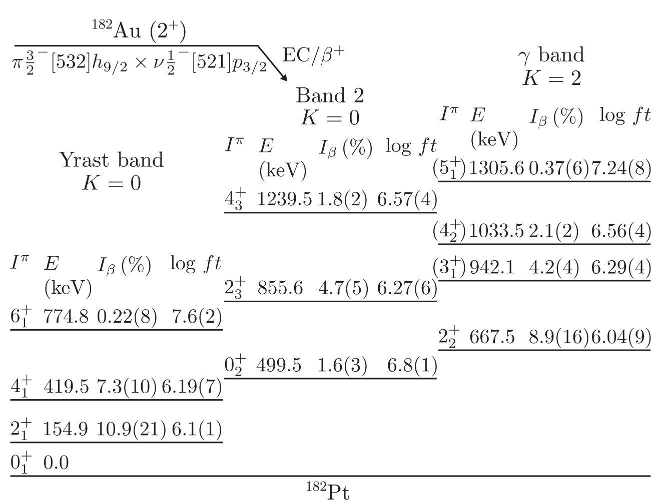

FIG. 13. Simplified level scheme of ^{182}Pt. The band structure is taken from Ref. [36]. Proton-neutron configuration of the ^{182}Au g.s. is taken from Ref. [6].

$Q_\beta - E_f$ [$Q_{EC}(^{182}Au) = 7864(23)$ keV] [52] for β decays to these levels.

V. CONCLUSION

We report the new results from decay spectroscopy of ^{182}Au performed at the ISOLDE Decay Station. The excited states in ^{182}Pt populated in ^{182}Au EC/β^+ decay were studied by the γ-γ coincidence method. A half-life value of $T_{1/2} = 16.43(12)$ s was obtained for ^{182}Au, which agrees within 2σ with the literature value $T_{1/2} = 15.5(4)$ s [32] and has a better precision. The ^{182}Pt level scheme was extended, where 125 new levels and 336 transitions were identified. Internal conversion coefficients for three transitions were determined, including the previously assumed $E0$ transition with the energy of 455 keV, for which γ rays were observed for the first time. The β-decay feeding intensities were evaluated, and a substantial feeding of the 4^+ states was observed. The $I = 3$ assignment for the ^{182}Au g.s. and the presence of a new $I = 5$ isomeric state were discussed as possible explanations, but they were rejected. Therefore, the influence of the pandemonium effect was assumed to be the main source of the observed feeding to the 4^+ states. Log ft values for decays into 2^+ states of different band structures in ^{182}Pt are the same within uncertainties, which indicates mixing between these bands. The α-decay branching ratio of $b_\alpha(^{182}Au) = 0.129(11)\%$ was determined and two new fine structure α decays feeding new levels in ^{178}Ir were observed. Based on the calculated conversion coefficient of the 55-keV transition, $I^\pi = (1^+, 2^+, 3^+)$ assignment for the ^{178}Ir g.s. was proposed.

ACKNOWLEDGMENTS

We acknowledge the support of the ISOLDE Collaboration and technical teams. This work was supported by the Slovak grant agency VEGA (Contract No. 1/0019/25); by the Slovak Research and Development Agency (Contracts No. APVV-18-0268 and No. APVV-22-0282); by the UK Science and Technology Facilities Council (Grants No. ST/P004598/1, No. ST/V001027/1, and No. ST/Y000242/1); by the FWO (Belgium) and F.R.S.-FNRS (Belgium) under the Excellence Of Science (EOS) program (Grants No. 30468642 and No. 40007501); by the Research Foundation Flanders under Projects No. I002619N, No. I002919N, and No. I012420N of the International Research Infrastructure; by the KU Leuven BOF (C14/22/104); by the FWO fellowship for fundamental research (Contract No. 1167324N); by the Spanish MCIN/AEI/10.13039/501100011033 under Grants No. PID2022-140162NB-I00, No. RTI2018-098868-B-I00, and No. PID2021-126998OB-I00; by Grupo de Fisica Nuclear (910059) at Universidad Complutense de Madrid; by the Polish Ministry of Science and Higher Education under Contract No. 2021/WK/07; by the Polish National Science Center under Grant No. 2020/39/B/ST2/02346; by the Romanian IFA grant CERN/ISOLDE and Nucleu Project No. PN 23 21 01 02; and by the German BMBF under Contract No. 05P21PKCI1 and Verbundprojekt 05P2021. A. N. Andreyev is grateful for support from the Chinese Academy of Sciences President's International Fellowship Initiative (Grant No. 2020VMA0017). M. Stryjczyk acknowledges funding from the European Union's Horizon 2020 research and innovation programme under Grant Agreement No. 771036 (ERC CoG MAIDEN).

DATA AVAILABILITY

The data that support the findings of this article are not publicly available. The data are available from the authors upon reasonable request.

[1] K. Wallmeroth, G. Bollen, A. Dohn, P. Egelhof, J. Grüner, F. Lindenlauf, U. Krönert, J. Campos, A. Rodriguez Yunta, M. J. G. Borge, A. Venugopalan, J. L. Wood, R. B. Moore, and H. J. Kluge, Phys. Rev. Lett. **58**, 1516 (1987).

[2] K. Wallmeroth, G. Bollen, A. Dohn, P. Egelhof, U. Krönert, M. Borge, J. Campos, A. Yunta, K. Heyde, C. De Coster, J. Wood, and H.-J. Kluge, Nucl. Phys. A **493**, 224 (1989).

[3] U. Krönert, S. Becker, G. Bollen, M. Gerber, T. Hilberath, H. J. Kluge, G. Passler *et al.* (ISOLDE Collaboration), Z. Phys. A **331**, 521 (1988).

[4] F. Le Blanc, J. Obert, J. Oms, J. C. Putaux, B. Roussière, J. Sauvage, J. Pinard, L. Cabaret, H. T. Duong, G. Huber, M. Krieg, V. Sebastian, J. Crawford, J. K. P. Lee, J. Genevey, and F. Ibrahim *et al.* (ISOLDE Collaboration), Phys. Rev. Lett. **79**, 2213 (1997).

[5] J. Cubiss, A. Barzakh, A. Andreyev, M. Al Monthery, N. Althubiti, B. Andel, S. Antalic, D. Atanasov, K. Blaum, T. Cocolios, T. Day Goodacre, R. de Groote, A. de Roubin, G. Farooq-Smith, D. Fedorov, V. Fedosseev, R. Ferrer, D. Fink, L. Gaffney, L. Ghys, A. Gredley, R. Harding, F. Herfurth, M. Huyse, N. Imai, D. Joss, U. Köster, S. Kreim, V. Liberati, D. Lunney, K. Lynch, V. Manea, B. Marsh, Y. Martinez Palenzuela, P. Molkanov, P. Mosat, D. Neidherr, G. O'Neill, R. Page, T. Procter, E. Rapisarda, M. Rosenbusch, S. Rothe, K. Sandhu, L. Schweikhard, M. Seliverstov, S. Sels, P. Spagnoletti, V. Truesdale, C. Van Beveren, P. Van Duppen, M. Veinhard, M. Venhart, M. Veselský, F. Wearing, A. Welker, F. Wienholtz, R. Wolf, S. Zemlyanoy, and K. Zuber, Phys. Lett. B **786**, 355 (2018).

[6] R. D. Harding, A. N. Andreyev, A. E. Barzakh, D. Atanasov, J. G. Cubiss, P. Van Duppen, M. Al Monthery, N. A. Althubiti, B. Andel, S. Antalic, K. Blaum, T. E. Cocolios, T. Day Goodacre, A. de Roubin, G. J. Farooq-Smith, D. V. Fedorov, V. N. Fedosseev, D. A. Fink, L. P. Gaffney, L. Ghys, D. T. Joss, F. Herfurth, M. Huyse, N. Imai, S. Kreim, D. Lunney, K. M. Lynch, V. Manea, B. A. Marsh, Y. Martinez Palenzuela, P. L. Molkanov, D. Neidherr, R. D. Page, A. Pastore, M. Rosenbusch, R. E. Rossel, S. Rothe, L. Schweikhard, M. D. Seliverstov, S. Sels, C. Van Beveren, E. Verstraelen, A. Welker, F. Wienholtz, R. N. Wolf, and K. Zuber, Phys. Rev. C **102**, 024312 (2020).

[7] J. G. Cubiss, A. N. Andreyev, A. E. Barzakh, V. Manea, M. A. Monthery, N. A. Althubiti, B. Andel, S. Antalic, D. Atanasov,

K. Blaum, T. E. Cocolios, T. D. Goodacre, A. de Roubin, G. J. Farooq-Smith, D. V. Fedorov, V. N. Fedosseev, D. A. Fink, L. P. Gaffney, L. Ghys, R. D. Harding, F. Herfurth, M. Huyse, N. Imai, D. T. Joss, S. Kreim, D. Lunney, K. M. Lynch, B. A. Marsh, Y. M. Palenzuela, P. L. Molkanov, D. Neidherr, G. G. O'Neill, R. D. Page, M. Rosenbusch, R. E. Rossel, S. Rothe, L. Schweikhard, M. D. Seliverstov, S. Sels, A. Stott, C. Van Beveren, P. Van Duppen, E. Verstraelen, A. Welker, F. Wienholtz, R. N. Wolf, and K. Zuber, Phys. Rev. C **102**, 044332 (2020).

[8] R. D. Harding, A. N. Andreyev, A. E. Barzakh, J. G. Cubiss, P. Van Duppen, M. Al Monthery, N. A. Althubiti, B. Andel, S. Antalic, T. E. Cocolios, T. D. Goodacre, K. Dockx, G. J. Farooq-Smith, D. V. Fedorov, V. N. Fedosseev, D. A. Fink, L. P. Gaffney, L. Ghys, J. D. Johnson, D. T. Joss, M. Huyse, N. Imai, K. M. Lynch, B. A. Marsh, Y. Martinez Palenzuela, P. L. Molkanov, G. G. O'Neill, R. D. Page, R. E. Rossel, S. Rothe, M. D. Seliverstov, S. Sels, C. Van Beveren, and E. Verstraelen, Phys. Rev. C **104**, 024326 (2021).

[9] J. G. Cubiss, A. N. Andreyev, A. E. Barzakh, P. Van Duppen, S. Hilaire, S. Péru, S. Goriely, M. Al Monthery, N. A. Althubiti, B. Andel, S. Antalic, D. Atanasov, K. Blaum, T. E. Cocolios, T. Day Goodacre, A. de Roubin, G. J. Farooq-Smith, D. V. Fedorov, V. N. Fedosseev, D. A. Fink, L. P. Gaffney, L. Ghys, R. D. Harding, M. Huyse, N. Imai, D. T. Joss, S. Kreim, D. Lunney, K. M. Lynch, V. Manea, B. A. Marsh, Y. Martinez Palenzuela, P. L. Molkanov, D. Neidherr, G. G. O'Neill, R. D. Page, S. D. Prosnyak, M. Rosenbusch, R. E. Rossel, S. Rothe, L. Schweikhard, M. D. Seliverstov, S. Sels, L. V. Skripnikov, A. Stott, C. Van Beveren, E. Verstraelen, A. Welker, F. Wienholtz, R. N. Wolf, and K. Zuber, Phys. Rev. Lett. **131**, 202501 (2023).

[10] A. Larabee, M. Carpenter, L. Riedinger, L. Courtney, J. Waddington, V. Janzen, W. Nazarewicz, J.-Y. Zhang, R. Bengtsson, and G. Lèander, Phys. Lett. B **169**, 21 (1986).

[11] W. F. Mueller, H. Q. Jin, J. M. Lewis, W. Reviol, L. L. Riedinger, M. P. Carpenter, C. Baktash, J. D. Garrett, N. R. Johnson, I. Y. Lee, F. K. McGowan, C. H. Yu, and S. Cwiok, Phys. Rev. C **59**, 2009 (1999).

[12] M. Venhart, M. Balogh, A. Herzáň, J. Wood, F. Ali, D. Joss, A. Andreyev, K. Auranen, R. Carroll, M. Drummond, J. Easton, P. Greenlees, T. Grahn, A. Gredley, J. Henderson, U. Jakobsson, R. Julin, S. Juutinen, J. Konki, E. Lawrie, M. Leino, V. Matoušek, C. McPeake, D. O'Donnell, R. Page, J. Pakarinen, P. Papadakis, J. Partanen, P. Peura, P. Rahkila, P. Ruotsalainen, M. Sandzelius, J. Sarén, B. Saygı, M. Sedlák, C. Scholey, J. Sorri, S. Stolze, A. Thornthwaite, R. Urban, J. Uusitalo, M. Veselský, and F. Wearing, Phys. Lett. B **806**, 135488 (2020).

[13] M. Venhart, J. L. Wood, M. Sedlák, M. Balogh, M. Bírová, A. J. Boston, T. E. Cocolios, L. J. Harkness-Brennan, R.-D. Herzberg, L. Holub, D. T. Joss, D. S. Judson, J. Kliman, J. Klimo, L. Krupa, J. Lušnák, L. Makhathini, V. Matoušek, Š. Motyčák, R. D. Page, A. Patel, K. Petrík, A. V. Podshibyakin, P. M. Prajapati, A. M. Rodin, A. Špaček, R. Urban, C. Unsworth, and M. Veselský, J. Phys. G **44**, 074003 (2017).

[14] M. Venhart, A. N. Andreyev, J. G. Cubiss, J. L. Wood, A. E. Barzakh, C. Van Beveren, T. E. Cocolios, R. P. de Groote, D. V. Fedorov, V. N. Fedosseev, R. Ferrer, D. A. Fink, L. Ghys, M. Huyse, U. Köster, J. Lane, V. Liberati, K. M. Lynch, B. A. Marsh, P. L. Molkanov, T. J. Procter, E. Rapisarda, K. Sandhu, M. D. Seliverstov, A. M. Sjödin, P. Van Duppen, and M. Veselský, Phys. Rev. C **105**, 034338 (2022).

[15] M. Sedlák, M. Venhart, J. L. Wood, V. Matoušek, M. Balogh, A. J. Boston, T. E. Cocolios, L. J. Harkness-Brennan, R.-D. Herzberg, D. T. Joss, D. S. Judson, J. Kliman, R. D. Page, A. Patel, K. Petrík, and M. Veselský, Eur. Phys. J. A **56**, 161 (2020).

[16] M. Balogh, E. Jajčišinová, M. Venhart, A. Herzáň, J. L. Wood, D. T. Joss, F. A. Ali, K. Auranen, S. Bánovská, M. Bírová, R. J. Carroll, D. M. Cox, J. G. Cubiss, T. Davis, M. C. Drummond, P. T. Greenlees, T. Grahn, A. Gredley, J. Henderson, U. Jakobsson, R. Julin, S. Juutinen, G. Kantay, J. Konki, P. Konopka, M. Leino, V. Matoušek, A. K. Mistry, C. G. McPeake, D. O'Donnell, R. D. Page, J. Pakarinen, P. Papadakis, J. Partanen, P. Peura, P. Rahkila, P. Ruotsalainen, M. Sandzelius, J. Sarén, B. Saygı, M. Sedlák, D. Seweryniak, C. Scholey, J. Sorri, A. Špaček, S. Stolze, M. Taylor, A. Thornthwaite, J. Uusitalo, M. Veselský, S. Vielhauer, and F. P. Wearing, Phys. Rev. C **106**, 064324 (2022).

[17] K. Heyde, J. D. Beule, B. Decroix, and C. D. Coster, Hyperfine Interact. **127**, 65 (2000).

[18] K. Heyde and J. L. Wood, Rev. Mod. Phys. **83**, 1467 (2011).

[19] P. E. Garrett, M. Zielińska, and E. Clément, Prog. Part. Nucl. Phys. **124**, 103931 (2022).

[20] F. G. Kondev, M. P. Carpenter, R. V. F. Janssens, I. Wiedenhöver, M. Alcorta, L. T. Brown, C. N. Davids, T. L. Khoo, T. Lauritsen, C. J. Lister, D. Seweryniak, S. Siem, A. A. Sonzogni, J. Uusitalo, P. Bhattacharyya, S. M. Fischer, W. Reviol, L. L. Riedinger, and R. Nouicer, Phys. Rev. C **61**, 044323 (2000).

[21] M. De Voigt, R. Kaczarowski, H. Riezebos, R. Noorman, J. Bacelar, M. Deleplanque, R. Diamond, F. Stephens, J. Sauvage, and B. Roussière, Nucl. Phys. A **507**, 472 (1990).

[22] D. G. Popescu, J. C. Waddington, J. A. Cameron, J. K. Johansson, N. C. Schmeing, W. Schmitz, M. P. Carpenter, V. P. Janzen, J. Nyberg, L. L. Riedinger, H. Hübel, G. Kajrys, S. Monaro, S. Pilotte, C. Bourgeois, N. Perrin, H. Sergolle, D. Hojman, and A. Korichi, Phys. Rev. C **55**, 1175 (1997).

[23] M. Carpenter, C. Bingham, L. Courtney, V. Janzen, A. Larabee, Z.-M. Liu, L. Riedinger, W. Schmitz, R. Bengtsson, T. Bengtsson, W. Nazarewicz, J.-Y. Zhang, J. Johansson, D. Popescu, J. Waddington, C. Baktash, M. Halbert, N. Johnson, I. Lee, Y. Schutz, J. Nyberg, A. Johnson, R. Wyss, J. Dubuc, G. Kajrys, S. Monaro, S. Pilotte, K. Honkanen, D. Sarantites, and D. Haenni, Nucl. Phys. A **513**, 125 (1990).

[24] G. Hebbinghaus, W. Gast, A. K. imer Flecken, R. Lieder, J. Skalski, and W. Urban, Z. Phys. A **328**, 387 (1987).

[25] G. Hebbinghaus, T. Kutsarova, W. Cast, A. Krämer-Flecken, R. Lieder, and W. Urban, Nucl. Phys. A **514**, 225 (1990).

[26] P. Hansen, H. Nielsen, K. Wilsky, M. Alpsten, M. Finger, A. Lindahl, R. Naumann, and O. Nielsen, Nucl. Phys. A **148**, 249 (1970).

[27] M. Finger, R. Foucher, J. Husson, J. Jastrzebski, A. Johnson, G. Astner, B. Erdal, A. Kjelberg, P. Patzelt, A. Hoglund, S. Malmskog, and R. Henck, Nucl. Phys. A **188**, 369 (1972).

[28] M. Cailliau, R. Foucher, J. Husson, and J. Letessier, J. Phys. Lett. **35**, 233 (1974).

[29] J. P. Husson, R. Foucher, A. Knipper, G. Klotz, G. Walter, C. F. Liang, and C. Richard-Serre (ISOLDE Collaboration), Proc. Int. Conf. Nuclei Far from Stability **A85**, 460 (1976).

[30] C. R. Bingham, M. B. Kassim, M. Zhang, Y. A. Akovali, K. S. Toth, W. D. Hamilton, H. K. Carter, J. Kormicki, J. von Schwarzenberg, and M. M. Jarrio, Phys. Rev. C **51**, 125 (1995).

[31] E. Hagberg, P. Hansen, P. Hornshøj, B. Jonson, S. Mattsson, and P. Tidemand-Petersson, Nucl. Phys. A **318**, 29 (1979).
[32] B. Singh, Nucl. Data Sheets **130**, 21 (2015).
[33] I. Romanski, I. Berkes, D. E. Brown, M. D. Jesus, R. Eder, I. S. Grant, E. Hagn, P. Harding, P. Herzog, B. Hinfurtner, B. Kastelein, H. Postma, J. Prinz, P. Richards, K. Schlösser, N. J. Stone, L. Vanneste, E. Zech *et al.* (NICOLE Collaboration and ISOLDE Collaboration), Hyperfine Interact. **75**, 457 (1992).
[34] F. Ibrahim, J. Genevey, E. Cottereau, A. Gizon, A. Knipper, F. Le Blanc, G. Marguier, J. Obert, J. Oms, J. C. Putaux, B. Roussière, J. Sauvage, A. Wojtasiewicz *et al.* (ISOLDE Collaboration), Eur. Phys. J. A **10**, 139 (2001).
[35] F. Kondev, M. Wang, W. Huang, S. Naimi, and G. Audi, Chin. Phys. C **45**, 030001 (2021).
[36] P. M. Davidson, G. D. Dracoulis, T. Kibédi, A. P. Byrne, S. Anderssen, A. Baxter, B. Fabricius, G. Lane, and A. Stuchbery, Nucl. Phys. A **657**, 219 (1999).
[37] M. J. G. Borge and B. Jonson, J. Phys. G **44**, 044011 (2017).
[38] V. Fedosseev, K. Chrysalidis, T. D. Goodacre, B. Marsh, S. Rothe, C. Seiffert, and K. Wendt, J. Phys. G **44**, 084006 (2017).
[39] ISOLDE Decay Station, https://isolde-ids.web.cern.ch/.
[40] See Supplemental Material at http://link.aps.org/supplemental/10.1103/rf8d-v286 for additional tables and figures.
[41] XIA Pixie-16, https://xia.com/support/pixie-16/.
[42] E. Rapisarda, A. N. Andreyev, S. Antalic, A. Barzakh, T. E. Cocolios, I. G. Darby, R. D. Groote, H. D. Witte, J. Diriken, J. Elseviers, D. Fedorov, V. N. Fedosseev, R. Ferrer, M. Huyse, Z. Kalaninová, U. Köster, J. Lane, V. Liberati, K. M. Lynch, B. A. Marsh, P. L. Molkanov, D. Pauwels, T. J. Procter, D. Radulov, K. Sandhu, M. D. Seliverstov, C. V. Beveren, P. V. den Bergh, P. V. Duppen, M. Venhart, M. Veselský, and K. Wrzosek-Lipska, J. Phys. G **44**, 074001 (2017).
[43] J. Chen, Nucl. Data Sheets **140**, 1 (2017).
[44] S. Zhu and E. McCutchan, Nucl. Data Sheets **175**, 1 (2021).
[45] M. Martin, Nucl. Data Sheets **108**, 1583 (2007).
[46] T. Kibédi Jr., T. Burrows, M. Trzhaskovskaya, P. Davidson, and C. Nestor, Nucl. Instrum. Methods A **589**, 202 (2008).
[47] B. Singh and J. C. Roediger, Nucl. Data Sheets **111**, 2081 (2010).
[48] Y. Xu, K. S. Krane, M. A. Gummin, M. Jarrio, J. L. Wood, E. F. Zganjar, and H. K. Carter, Phys. Rev. Lett. **68**, 3853 (1992).
[49] J. Dowie, T. Kibédi, T. Eriksen, and A. Stuchbery, At. Data Nucl. Data Tables **131**, 101283 (2020).
[50] S. Turkat, X. Mougeot, B. Singh, and K. Zuber, At. Data Nucl. Data Tables **152**, 101584 (2023).
[51] NNDC log *ft* calculator, https://www.nndc.bnl.gov/logft/.
[52] M. Wang, W. Huang, F. Kondev, G. Audi, and S. Naimi, Chin. Phys. C **45**, 030003 (2021).
[53] J. Hardy, L. Carraz, B. Jonson, and P. Hansen, Phys. Lett. B **71**, 307 (1977).
[54] F. Meissner, H. Salewski, W.-D. Schmidt-Ott, U. Bosch-Wicke, V. Kunze, and R. Michaelsen, Phys. Rev. C **48**, 2089 (1993).
[55] R. B. Firestone, V. S. Shirley, C. Baglin, S. Chu, and J. Zipkin, *Table of Isotopes*, 8 ed. (John Wiley & Sons, New York, 1996).
[56] J. O. Rasmussen, Phys. Rev. **113**, 1593 (1959).
[57] F. Kondev, Nucl. Data Sheets **159**, 1 (2019).
[58] C. M. Baglin, Nucl. Data Sheets **110**, 265 (2009).
[59] A. Siivola, Nucl. Phys. **84**, 385 (1966).
[60] X. Yang (private communication, 2024).
[61] F. R. Xu, P. M. Walker, J. A. Sheikh, and R. Wyss, Phys. Lett. B **435**, 257 (1998).
[62] W. Nazarewicz, J. Dudek, R. Bengtsson, T. Bengtsson, and I. Ragnarsson, Nucl. Phys. A **435**, 397 (1985).
[63] J. Dudek, Z. Szymański, and T. Werner, Phys. Rev. C **23**, 920 (1981).
[64] W. D. Myers and W. Swiatecki, Ann. Phys. **55**, 395 (1969).
[65] V. Strutinsky, Nucl. Phys. A **95**, 420 (1967).
[66] H. Pradhan, Y. Nogami, and J. Law, Nucl. Phys. A **201**, 357 (1973).
[67] P. Möller and J. Nix, Nucl. Phys. A **536**, 20 (1992).
[68] Y. H. Zhang, Y. D. Fang, G. de Angelis, N. Marginean, A. Gadea, D. R. Napoli, M. Axiotis, C. Rusu, T. Martinez, H. L. Wang, X. H. Zhou, W. T. Guo, M. L. Liu, Y. X. Guo, X. G. Lei, M. Oshima, and Y. Toh, Phys. Rev. C **70**, 057303 (2004).
[69] C. M. Baglin, Nucl. Data Sheets **111**, 275 (2010).
[70] S. Kreim *et al.* (ISOLTRAP Collaboration) (private communication, 2012).
[71] P. Hornshøj, B. Erdal, P. Hansen, B. Jonson, K. Aleklett, and G. Nyman, Nucl. Phys. A **239**, 15 (1975).
[72] P. Walker and F. Kondev, Eur. Phys. J. Spec. Top. **233**, 983 (2024).